



## RESEARCH ARTICLE

# Multiple cell types in the oviduct express the prolactin receptor

Kelly C. Radecki<sup>1</sup> | Matthew J. Ford<sup>2</sup> | Hollian R. Phillipps<sup>3</sup> | Mary Y. Lorenson<sup>1</sup> | David R. Grattan<sup>3</sup>  | Yojiro Yamanaka<sup>2</sup> | Ameae M. Walker<sup>1</sup> 

<sup>1</sup>Division of Biomedical Sciences, School of Medicine, University of California, Riverside, California, USA

<sup>2</sup>Department of Human Genetics, Rosalind and Morris Goodman Cancer Institute, McGill University, Quebec, Canada

<sup>3</sup>Centre for Neuroendocrinology and Department of Anatomy, School of Biomedical Sciences, University of Otago, Dunedin, New Zealand

## Correspondence

Ameae M. Walker, Division of Biomedical Sciences, 1255 Webber Hall, School of Medicine, University of California, Riverside, CA 92521, USA.  
Email: [ameae.walker@ucr.edu](mailto:ameae.walker@ucr.edu)

## Funding information

National Institutes of Health, Grant/Award Number: 1S10OD021718-01, 1S10OD010794-01 and 1S10RR025496-01; Cancer Center Support, Grant/Award Number: P30CA-062203; University of California, Irvine; Neurological Foundation of New Zealand; FRQS; CRRD; Canderel; Pease Cancer and Mary Galvin Burden Pre-Doctoral Fellowships

## Abstract

Little is known about the physiological role of prolactin in the oviduct. Examining mRNA for all four isoforms of the prolactin receptor (PRLR) in mice by functional oviduct segment and stage of the estrous cycle, we found short form 3 (SF3) to be the most highly expressed, far exceeding the long form (LF) in highly ciliated areas such as the infundibulum, whereas in areas of low ciliation, the SF3 to LF ratio was ~1. SF2 expression was low throughout the oviduct, and SF1 was undetectable. Only in the infundibulum did PRLR ratios change with the estrous cycle. Immunofluorescent localization of SF3 and LF showed an epithelial (both mucosal and mesothelial) distribution aligned with the mRNA results. Despite the high SF3/LF ratio in densely ciliated regions, these regions responded to an acute elevation of prolactin (30 min, intraperitoneal), with LF-tyrosine phosphorylated STAT5 seen within cilia. Collectively, these results show ciliated cells are responsive to prolactin and suggest that prolactin regulates estrous cyclic changes in ciliated cell function in the infundibulum. Changes in gene expression in the infundibulum after prolonged prolactin treatment (7-day) showed prolactin-induced downregulation of genes necessary for cilium development/function, a result supporting localization of PRLRs on ciliated cells, and one further suggesting hyperprolactinemia would negatively impact ciliated cell function and therefore fertility. Flow cytometry, single-cell RNAseq, and analysis of LF-td-Tomato transgenic mice supported expression of PRLRs in at least a proportion of epithelial cells while also hinting at additional roles for prolactin in smooth muscle and other stromal cells.

## KEYWORDS

cilia, estrous cycle, gene expression profiling, hyperprolactinemia, prolactin, receptors

**Abbreviations:** hPRL, human prolactin; LF, long form of the prolactin receptor; LF-td-Tomato transgenic mouse, mouse expressing td-tomato wherever long form prolactin receptor has been expressed; mPRL, mouse prolactin; PRL, prolactin; PRLR, prolactin receptor; RankL, Receptor activator of nuclear factor kappa-B ligand; SF1-3, short forms of the prolactin receptor 1-3; STAT5, signal transducer and activator of transcription 5.

This is an open access article under the terms of the [Creative Commons Attribution-NonCommercial-NoDerivs](https://creativecommons.org/licenses/by-nc-nd/4.0/) License, which permits use and distribution in any medium, provided the original work is properly cited, the use is non-commercial and no modifications or adaptations are made.

© 2022 The Authors. *FASEB BioAdvances* published by Wiley Periodicals LLC on behalf of The Federation of American Societies for Experimental Biology.

## 1 | INTRODUCTION

The murine oviduct is similar in function and morphology to the human fallopian tube and consists of four classically recognized segments: the infundibulum, ampulla, isthmus, and utero-tubal junction. The mucosal epithelium is pseudostratified, encompassing both multi-ciliated and secretory cells. The mucosal epithelium of the infundibulum is the most densely ciliated, whereas that of the isthmus contains the most secretory cells. Unlike the human fallopian tube, the murine oviduct is a coiled structure, supported by the mesosalpinx, an extension of the broad ligament peritoneum. The infundibulum receives the ova, the ampulla is the location of fertilization, and developing embryos then pass into the isthmus before entering the uterus.<sup>1,2</sup>

Several isoforms of the PRLR have been identified in rodents and humans, with mice and humans producing one long and three shorter isoforms.<sup>3–5</sup> These PRLR isoforms are produced by alternative splicing of the same PRLR pre-mRNA. The long and short isoforms each have exons 3–9, encoding identical extracellular and transmembrane domains.<sup>5,6</sup> The long form (LF) PRLR incorporates exon 10, while the short forms (SFs) lack this particular exon and substitute other exons or portions thereof, depending on species. These differences in 3' splicing, contribute to differences in intracellular signaling by the translated protein. For example, only the LF PRLR has the ability to recruit signal transducer and activator of transcription 5 (STAT5), which is then tyrosine phosphorylated by Janus kinase 2.<sup>6</sup> Although originally and still often described to act only as dominant negatives for signaling through the LF, some of the SFs in mice and humans have been determined to have distinct signaling pathways.<sup>7–11</sup>

The hypothesis that prolactin (PRL) may have a role/s in the oviduct derives from analysis of the PRLR null mouse. In this mouse, although ova were viable and recoverable from knockout animals, there was an arrest of preimplantation development. Proper development required placement of ova from PRLR null females into oviducts of PRLR +/+ foster mothers.<sup>12</sup> In addition, when PRLR null females were mated with PRLR+/+ males, there were reduced fertilization rates.<sup>12</sup> While these effects could be indirect, they suggested the possibility that loss of the PRLR from the oviduct could result in an abnormal environment for ovum transport, fertilization in the ampulla or preimplantation development in the ampulla and isthmus. The possibility of a direct role for PRL in the oviduct has been strengthened by PRLR immunolocalization to the mucosal epithelium in human and mouse oviducts<sup>13</sup> and by smooth muscle expression of LF PRLR in a transgenic *Prlr*-IRES-Cre reporter mouse.<sup>14</sup> Most circulating

PRL is produced by lactotrophs in the anterior pituitary. However, many other tissues produce smaller quantities of PRL, express the prolactin receptor (PRLR) and often use PRL in an autocrine/paracrine fashion.<sup>12,15,16</sup> PRL is elevated during proestrus in mice, and stimulated by mating to be high in early pregnancy such that plasma PRL levels are elevated throughout the periovulatory period as the oocyte or preimplantation embryo is transported through the oviduct.<sup>17,18</sup>

Here, we have built on this very limited previous information and show PRLR quantity and isoform expression differences by functional oviduct segment and cell type, estrous cycle regulation of PRLRs in the infundibulum, and evidence that PRL affects multi-ciliated cells.

## 2 | MATERIALS AND METHODS

### 2.1 | Animals

Young adult female C57BL6/J mice were obtained from Jackson Laboratories at 6 weeks of age, housed with 12h:12h light:dark cycles and fed standard chow, ad libitum. All procedures were approved by the University of California, Riverside Institutional Animal Care and Use Committee. When treatment groups were compared, mice were randomly assigned, coded for blind analysis and housed together. For PRLR mRNA and histological analyses, animals were subjected to vaginal smearing<sup>19</sup> between 11am and 12pm daily to determine the stage of the estrous cycle for up to 3 weeks prior to sacrifice. The oviduct was micro-dissected for the harvest of the infundibular, ampullary, and isthmus segments, as described previously.<sup>20</sup> For in vivo STAT5 phosphorylation experiments, diestrus animals were treated with recombinant human PRL (hPRL), prepared, quality assessed, and quantified as previously described,<sup>21</sup> administered at 5 µg/g in Dulbecco's phosphate buffered saline (DPBS) intraperitoneally (IP). Oviducts were harvested after 30 min and fixed (see below). For RNA sequencing (RNAseq), animals were treated with recombinant murine PRL (mPRL) (purchased from Dr. Albert Parlow, Lundquist Institute). The mPRL was initially dissolved in 0.01 M sodium bicarbonate, pH 9.2, and then diluted in DPBS to pH 8. Animals were treated via subcutaneous Alzet osmotic minipump (#2001, Durect, Cupertino) at 3 µg/h/mouse for 7 days, which approximately doubled the median circulating PRL (Figure S1) at proestrus, as assessed by Nb2 bioassay, conducted as previously described.<sup>22</sup> Infundibula were dissected and immediately snap frozen in liquid N<sub>2</sub> for RNA extraction. To verify treatment efficacy, mammary glands were processed for RT-qPCR detection of RankL and Cyclin D1 expression.<sup>23</sup>

## 2.2 | Transgenic animals

Adult female LF *Prlr*-IRES-Cre crossed with a B6.Cg-*Gt(ROSA)26Sor<sup>tm9(CAG-tdTomato)Hze</sup>/J* (Jackson Laboratory, 007909) reporter mouse line, LF *Prlr*-IRES-Cre td-Tomato ( $n = 8$ ) aged 8–10 weeks, were obtained from the University of Otago's colony housed at the Taieri Resource Unit. These mice are an LF PRLR-specific reporter mouse line in which a construct containing an internal ribosome entry site (IRES) and Cre recombinase is inserted immediately following exon 10 of the *Prlr* gene to facilitate co-expression.<sup>14,24</sup> td-Tomato expression is visualized specifically in LF *Prlr*-expressing cells following Cre-mediated recombination, when the CAG promoter-driven construct located in the *Gt(ROSA)26Sor* locus is present in a cell also containing Cre recombinase. Mice were group-housed under standard conditions; room temperature set to  $22 \pm 1^\circ\text{C}$ , 12h:2h light:dark cycle and standard chow and water freely available at all times. Stages of the estrous cycle were monitored by a daily collection of vaginal smears for about 2 weeks and cytological examination of smears was used to identify each stage. All procedures involving LF *Prlr*-IRES-Cre td-Tomato mice were approved by the University of Otago Ethics Committee (AEC 20/93).

## 2.3 | RNA extraction

All tissues were homogenized in TRIzol (cat# 15596026, Invitrogen, Thermo Fisher) using stainless steel beads (1:1 cat# SSB05:SB4B, Next Advance), the homogenized tissue was eluted from the beads and carried through to

RNA precipitation as per the manufacturer's guidelines (Invitrogen). All samples were precipitated in two volumes of 100% isopropanol overnight at  $4^\circ\text{C}$ . RNA was purified on column using the Qiagen RNeasy Extraction Kit (cat# 74134, Qiagen, Germantown, MD, USA). Whole RNA was stored at  $-80^\circ\text{C}$  until reverse transcription. RNA quality was initially determined by NanoDrop OD 260/280 nm and 260/230 nm ratios and quantified by Qubit Fluorometer RNA Broad Range Assay Kit (cat# Q1020, Invitrogen). For RNAseq, RNA quality was further assessed with the 2100 Bioanalyzer system and only samples above 7.5 RNA integrity number were used (Agilent).

## 2.4 | Quantitative PCR

Primer sets were designed utilizing Primer BLAST (NCBI) and the OligoAnalyzer Tool available through Integrated DNA Technologies (IDT, San Diego, CA, USA) and manufactured by IDT. Primer sequences are listed in Table 1. Optimized primer conditions were used to generate standard curves to verify equivalent efficiency of reactions among primer sets (90%–110% efficiency, Figure S2). All primers used were found to be optimal at  $0.3 \mu\text{M}$  primer concentration and  $58^\circ\text{C}$  annealing temperature.

First-strand cDNA was reverse-transcribed using an oligo-dT primer (IDT) and Moloney Murine Leukemia Virus Reverse Transcriptase (M-MLVRT) (cat# M1701, Promega), according to the manufacturer's guidelines. cDNA was stored at  $-20^\circ\text{C}$  until analysis.

Melt curve analysis was performed in parallel with all qPCR protocols to confirm the specificity of the amplified

TABLE 1 Primer sequences used for qPCR

Gene	Primer sequence
LF <i>Prlr</i>	F: ATAAAAGGATTTGATACTCATCTGCTAGAG R: TGTCATCCACTCCAAGAACTCC
SF3 <i>Prlr</i>	F: TGCATCTTTCCACCAGTTCCGGGGC R: TTGTATTTGCTTGGAGAGCCAGT
SF2 <i>Prlr</i>	F: TGCATCTTTCCACCAGTTCCGGGGC R: TCAAGTTGCTCTTTGTTGTCAAC
SF1 <i>Prlr</i>	F: AAGCCAGACCATGGATACTGGAG R: AACTGGAGAATAGAACCAGAG
<i>Mcidas</i>	F: AACCGAAGCGTCTCCTAGTG R: GGTCATCCATTGCATCTCTG
<i>RankL</i>	F: CCAAGATCTCTAACATGACG R: CACCATCAGCTGAAGATAGT
<i>Cyclin D1</i>	F: CGCCCTCCGTATCTTACTTCAA R: CTCACAGACCTCCAGCATCCA
<i>Gapdh</i>	F: AACAGCAACTCCCCTCTTC R: CCTGTTGCTGTAGCCGTATT
Kidney thyroglobulin variant	F: CTACCATCTACAGGGAGGT R: GCTCTGCTCCTCCGTTGAAA

product. qPCR reactions were performed with 2X SYBR Green Supermix according to the manufacturer's guidelines (Bio-Rad) on a Bio-Rad CFX96 Real-Time PCR Detection System. All samples were run for 40 cycles with endogenous and no-template controls.

Cycle threshold (Ct) values were assessed for well-to-well deviation in triplicate with threshold standard deviation  $\leq 0.1$ . Average Ct values were normalized to endogenous control gene expression in the same animal ( $\Delta$ Ct) with sub-normalization to verify consistent expression of the endogenous control gene (i.e., endogenous control remains unchanged regardless of treatment group, estrous stage, etc.).  $\Delta$ Ct values were fold computed and normalized to a comparable group (i.e., control/untreated, set as 1) to generate  $\Delta\Delta$ Ct values as described by Livak and Schmittgen.<sup>25</sup>

## 2.5 | Antibodies

Antibodies and working parameters are in Table 2. Isoform-specific PRLR antibodies were originally developed by Dr. Patricia M. Ingleton, and what quantities remain are now in the care of Dr. Michael Symonds (University of Nottingham, UK). The antibodies were produced against peptide regions of rat liver PRLRs linked to thyroglobulin. Antiserum R122 was raised against residues 309–325, specific to the intracellular region of the LF (100% identity exists between the rat and mouse LF for this region). R133 was raised against residues 281–296, specific to the intracellular domain of the short rat receptor, which has 87% identity (100% for residues 281–290) to the mouse SF3, and no homology with the other two mice SFs. Neither of these sequences shares significant homology with other members of the cytokine receptor family or any other protein in the NCBI database. Specificity of the antibodies was determined by western blot analysis of PRLR negative cells without and with overexpression of the mouse PRLR isoforms.<sup>26</sup> Since the discovery of a truncated form of thyroglobulin expressed in the kidney,<sup>27</sup> an additional control for specificity included a determination by RT-qPCR that a similar form of truncated thyroglobulin was not expressed in the oviduct, and it was not.

## 2.6 | Histological preparation and immunostaining

Tissues were washed in DPBS and fixed in cold DPBS-buffered 4% paraformaldehyde (PFA, cat# 158127, Sigma-Aldrich) overnight at 4°C. Paraplast embedding, sectioning, and immunostaining were as described previously.<sup>26</sup> For analysis of STAT5 tyrosine phosphorylation,

cryosectioning was used and protease/phosphatase inhibitors were included in all solutions (Abcam # 201120). Fixed samples were cryoprotected in a series of sucrose incubations at 4°C and embedded in Optimal Cutting Temperature compound (Sakura). Frozen blocks were stored airtight at  $-80^{\circ}\text{C}$  until sectioning on a standard Cryostat (Leica, Buffalo Grove, IL, USA) and stored at  $-80^{\circ}\text{C}$  until staining within 24 h of sectioning.

Controls included the use of secondary antibody alone and checks for cross-reactivity of multiplexed secondary antibodies (Figure S3). After clearance of embedding medium, sections were permeabilized with 0.5% Triton-X-100 (v/v) in 1% (w/v) bovine serum albumin (BSA)/Tris-buffered saline with 0.1% (v/v) Tween (BTBST) for 15 min at room temperature and then blocked with animal sera (5% v/v), matched to species of the secondary antibody, in BTBST for 30 min at room temperature. Primary antibody was diluted in BTBST and incubated at 4°C overnight. Sections were washed between steps with BTBST. Secondary antibodies were diluted in BTBST and incubated for 2 h at room temperature. Sections were then additionally washed in DPBS, stained with Hoescht (1:2000, 33,342, Invitrogen) nuclear stain for 20 min at room temperature, mounted in ProLong Gold Antifade Reagent (cat# P10144, Life Technologies), and stored at 4°C until imaging.

## 2.7 | td-Tomato immunofluorescent staining

LF *Prlr*-IRES-Cre td-Tomato mice ( $n = 8$ ) in proestrus were deeply anesthetized with Pentobarbitone (100 mg/kg IP) prior to transcardial perfusion with 4% (w/v) PFA in 0.1 M phosphate buffer (pH 7.4). Oviducts were dissected with coiling retained and ovaries and a portion of the uterus also intact to maintain orientation, then post-fixed in 4% (w/v) PFA in 0.1 M phosphate buffer for 1 h. Tissue was stored in 70% (v/v) Ethanol prior to paraffin embedding. Sections (4  $\mu\text{m}$ ) were taken at 12  $\mu\text{m}$  intervals through the oviduct using a Leica RM2235 microtome and mounted onto FLEX IHC microscope slides (# K8020, Dako). Six sections containing all distinct regionalities of the oviduct were selected from each mouse for detection of *LF-Prlr*-expressing cells by immunofluorescent localization of td-Tomato. Sections were baked at 60°C for 5 min, dewaxed and rehydrated. After three washes in 0.05 M Tris-Buffered Saline (TBS), sections were incubated in blocking solution (0.05 M TBS, 0.3% (v/v) Triton X-100, 0.2% (w/v) BSA, 5% (v/v) normal donkey serum) for 2 h. Sections were washed, then incubated in a goat anti-td-Tomato polyclonal antibody diluted 1:1000 in blocking solution overnight at 4°C. Any remaining primary

TABLE 2 Antibodies and conditions

Antibody	Application	Host	Target Species	Clone	Manufacturer, Cat#	Dilution	Incubation
Anti-LF PRLR	IF	Rabbit	Rat/mouse	R122	N/A	1:100	4°C, O/N
Anti-SF3 PRLR	IF	Rabbit	Rat/mouse	R133	N/A	1:100	4°C, O/N
Anti-LF PRLR	FC	Rabbit	Rat/mouse	R122	N/A	1:1000	4°C, 1 h
Anti-SF3 PRLR	FC	Rabbit	Rat/mouse	R133	N/A	1:1000	4°C, 1 h
Anti-acetylated- $\alpha$ -tubulin	IF	Mouse	Mouse	611B1	Sigma, T7451	1:1000	4°C, O/N
Anti-acetylated- $\alpha$ -tubulin	IF	Rabbit	Mouse	EPR16772	Abcam, ab179484	1:1000	4°C, O/N
Anti-acetylated- $\alpha$ -tubulin Alexa Fluor 647	FC	Rabbit	Mouse	D20G3	Cell Signaling Technologies, 81502S	1:200	4°C, 1 h
Anti-pStat5	IF	Rabbit	Mouse	D47E7	Cell Signaling Technology, 4322S	1:100	4°C, O/N
Anti-CD45-APC/CY7	FC	Rat	Mouse	30-F11	Biologend, 103,116	1:1500	4°C, 1 h
Anti-tdTomato	IF	Goat	Red fluorescent protein (DsRed) from so-called disk corals of <i>Discosoma</i> species		Sicgen, AB8181-200	1:1000	4°C, O/N
Anti-EpCAM (CD326)- PerCP-Fluor 710	FC	Rat	Mouse	G8.8	eBioscience, 46-5791-82	1:600	4°C, 1 h
Anti-Rabbit-IgG Alexa Fluor 488	IF	Goat	Mouse		Invitrogen	1:1000	RT°C, 2 h
Anti-Mouse-IgG Alexa Fluor 488	IF	Goat	Rabbit		Invitrogen	1:1000	RT°C, 2 h
Anti-Rabbit-IgG Alexa Fluor 555	IF	Goat	Rabbit		Invitrogen	1:1000	RT°C, 2 h
Anti-Rabbit-IgG Alexa Fluor 647	IF	Goat	Rabbit		Invitrogen	1:1000	RT°C, 2 h
Anti-Rabbit-IgG Alexa Fluor 488	IF	Donkey	Goat		Invitrogen	1:500	RT°C, 2 h

Abbreviations: FC, flow cytometry; IF, immunofluorescence; N/A, not applicable; O/N, overnight; RT, room temperature.

antibody was removed by washing sections three times in 0.05 M TBS prior to incubation in Donkey anti-goat IgG Alexa Fluor 488 diluted 1:500 in blocking solution for 2 h at room temperature. Sections underwent a final three washes in 0.05 M TBS and coverslips were applied using Fluoromount-G™ Mounting Medium with DAPI (#00-4959-52, Thermo Fisher).

## 2.8 | Microscopy and image analysis

All images to be directly compared were acquired under equivalent and consistent parameters including objective lens, laser strength, pinhole, gain/offset, and export conditions. Microscopy controls checked for channel bleeding, and 3-D reconstruction and rotation determined sub-cellular location. Confocal images and z-stacks were acquired on an upright or inverted Zeiss 880 Confocal Microscope. Z-stack progressions were acquired through the thickness of the section and compressed as orthogonal projections utilizing ZEN Imaging Software (Zeiss). PRLR isoform localization images were also acquired with the Zeiss Airyscan high resolution detector on an inverted Zeiss 880 Confocal Microscope.<sup>28</sup> All images were exported as TIF files to preserve pixel integrity and, where specified, quantified with ImageJ Software (free download from <https://imagej.nih.gov/ij>). Quantification of STAT5 tyrosine phosphorylation is presented as mean gray value (MGV) per specified region of interest (ROI) (e.g., epithelium, smooth muscle) normalized to area of the ROI (MGV as a fraction of area). 3D rendered images were generated using Imaris Bitplane 3D visualization software (Bitplane, Zurich, CH). Images of LF detected via td-Tomato immunofluorescence were acquired on a Nikon Ti2E Widefield Brightfield and fluorescence microscope with associated NIS-Elements software (Nikon® Instruments Inc). Acquired ND2 formatted images were converted to TIF files and analyzed using ImageJ software.

## 2.9 | Dissociation of the oviduct

For flow cytometry, oviduct cells from 16 adult female mice were dissociated and pooled, as described previously.<sup>20</sup> Briefly, cells were nonenzymatically dissociated in DPBS containing 5 mM EDTA, 1 g/L glucose, and 0.4% (w/v) BSA at 37°C for 9–10 min with gentle pipetting every 3 min. This results in single cells plus some small cell clumps. The small clumps were then further dissociated by a 25–30 min incubation in 0.15% pronase (Roche Diagnostics) in 50:50 DMEM/Ham's F12 (Corning) at 4°C, again with gentle pipetting every 3 min. This protocol results in a preparation of cells (Figure S4) that is about

31% epithelial (EpCAM+) further subdivided into secretory (EpCAM+, acetylated tubulin-) and multi-ciliated (EpCAM+, acetylated tubulin+), 11% immune (CD45+), 8% epithelial-immune (EpCAM+, CD45+), and 50% stromal (EpCAM-,CD45-).

For single cell RNAseq, cells from a 3-month-old mouse in estrus were dissociated by incubation in collagenase B (5 mg/ml) and DNase I (5 U/100 µl) in Dulbecco's modified Eagle's medium containing 100 IU/mL of Penicillin and 100 µg/ml of Streptomycin (Gibco Thermo Fisher) for 35 min at 37°C followed by passage through a needle series.<sup>29</sup>

## 2.10 | Flow cytometry

Dissociated oviduct cells were fixed in DPBS-buffered 4% PFA, pH 7.4 for 5 min at room temperature, subjected to centrifugation at 500 g for 3 min, washed in FACS buffer (0.4% w/v BSA/50 mM EDTA in DPBS, pH 7.4) and then incubated in permeabilization buffer (0.1% v/v Triton-X-100 in FACS buffer) for 15 min at room temperature. Cells were pelleted again, washed in FACS buffer and incubated in Fc blocking buffer for 10 min at 4°C (1:100 in FACS buffer, Invitrogen). Primary or directly conjugated antibodies were added directly to Fc blocking buffer and incubated for 1 h at 4°C. Cells were then pelleted again and washed twice in FACS buffer for 5 min each and re-suspended in secondary antibody for 1 h at 4°C. Cells were then pelleted again and washed twice in FACS buffer for 5 min each and resuspended for immediate analysis on a BD FACS Canto II flow cytometer. Compensation was determined using UltraComp eBeads Plus (cat# 01-3333-42, Invitrogen) and results were analyzed with FlowJo software (BD Biosciences).

## 2.11 | Tissue RNAseq and analysis

Both infundibular regions were pooled per mouse and two animals were pooled for each RNAseq sample (four infundibula per sample, five samples per treatment). Whole transcriptome sequencing was performed using the Illumina NovaSeq 6000 system. Samples were enriched for mRNA (stranded) and sequenced by 100 base pair (bp) paired end (PE) reads (PE100, 80 million reads per sample). Reads were quality assessed using FastQC quality assessment software and trimmed using a quality threshold of 15 and Truseq adapter sequences (reads shorter than 20 bp were discarded, Trimmomatic). Reads were aligned to the mouse mm10 reference genome with a splice aware short read aligner (Hisat2, Samtools). FeatureCounts were used to quantify raw

counts and two group comparison, using DESeq2 to identify differentially expressed genes between control and PRL-treated animals. Differential transcript usage (DTU) analysis was performed using Salmon quantification.<sup>30</sup> Files have been uploaded to NCBI's GEO with accession # GSE199199.

## 2.12 | Single cell RNAseq

Single cell RNAseq analyzed a previously published dataset of mouse oviduct cells isolated from a single female during estrus.<sup>29</sup> Briefly, oviducts were enzymatically and mechanically dissociated as described above before the resultant cells were FAC sorted to isolate viable cells and enrich for epithelial populations (EpCAM+ CD45-). The single cell expression data were then generated according to the Chromium Single Cell 3' Reagent Kits User Guide (V2 Chemistry, 10X genomics) and sequenced on an Illumina HiSeq4000. Raw sequencing data for each sample were converted to matrices of expression counts using the Cell Ranger software provided by 10X genomics (version 2.0.2). Briefly, raw BCL files from the Illumina HiSeq were demultiplexed into paired-end, gzip-compressed FASTQ files for each channel using Cell 735 Ranger's mk-fastq. Using Cell Ranger's count, reads were aligned to the mouse reference transcriptome (mm10), and transcript counts quantified for each annotated gene within every cell. The resulting UMI count matrices (genes×cells) were then provided as input to Seurat suite (version 2.3.4). Cells were first filtered to remove those that contained fewer than 200 genes detected and those in which >10% of the transcript counts were derived from mitochondrial-740 encoded genes. Mean UMIs and genes detected in each cell were 3696 and 1546. Clustering was performed using the "FindClusters" function and Uniform Manifold Approximation and Projection (UMAP) visualization for all cells. Cluster-specific gene markers were identified using Seurat's FindMarkers with cutoffs avg logFC > 0.5 and FDR < 0.05. Nine distinct populations were identified by clustering and visualization by UMAP. Evaluation of the top differentially expressed genes identified populations of stromal (*Col1a1*, *Col3a1*, *Col1a2*), smooth muscle (*Acta2*), cumulus (*Cyp11a1*, *Sfrp4*), endothelial (blood) (*Pecam1*), multi-ciliated (*Foxj1*), secretory (*Ovgp1*), mesothelial (*Msln*, *Nkain4*), and endothelial (lymphatic) (*Prox1*) cells, and an unclassified cluster.

## 2.13 | Additional statistical analyses

For comparison of more than two groups, ANOVA was performed with Tukey's post hoc correction for multiple

comparisons. Comparison between two groups was performed with an unpaired *t*-test with one-tail analysis. When appropriate, Grubb's Outlier Test was applied.<sup>31</sup> All these analyses used Prism software (GraphPad), and a  $p < 0.05$  was considered significant.

## 3 | RESULTS

### 3.1 | Expression of PRLR isoforms

Because of differences in physiological function and susceptibility to pathological change among the three major segments of the oviduct, we examined mRNA expression of all four isoforms of the PRLR as a function of segment and stage of the estrous cycle (Figure 1A–F). SF3 was the most highly expressed isoform in the oviduct, followed by LF and then SF2. SF1 was undetectable. SF3 was most highly expressed in the infundibular region where the predominant cell type in the mucosal epithelium is multiciliated (Figure 1A). By contrast, the LF was most highly expressed in the isthmus (Figure 1C) where the majority cell type in the mucosal epithelium is secretory. Estrous cycle regulation of SF3 and LF only occurred in the infundibulum. The highest expression of SF3 occurred in diestrus and proestrus (Figure 1B) and the highest expression of LF was at proestrus (Figure 1D). SF2 was low and relatively stable (Figure 1E,F).

Because the SFs of the PRLR are often described as dominant negatives for the LF, and because the receptor ratio dictates downstream signaling, we were also interested in the LF/SF ratios of the isoforms (Figure 1G,H). The LF/SF3 ratio is significantly lower in the infundibulum as compared to the ampulla and isthmus, (Figure 1G) while the LF/SF2 ratio is similar throughout the oviduct (Figure 1H). The LF/SF3 and LF/SF2 ratios changed significantly with the estrous cycle only in the infundibulum (Figure 1G,H).

### 3.2 | Localization of PRLR

Using antibodies specific to the two most highly expressed forms of the PRLR, SF3, and LF, we found immunostaining to be in good general agreement with the mRNA results. Thus, SF3 was most highly expressed in densely ciliated areas and LF was most highly expressed in the isthmus (Figure 2). Of additional interest, we found substantial PRLR immunostaining of the mesothelium and that this followed the pattern on the mucosal epithelium, with SF3 highest on the mesothelium of the ampulla (mesothelium is absent in the infundibulum) and LF highest on the mesothelium in the isthmus region (Figure 2 shows

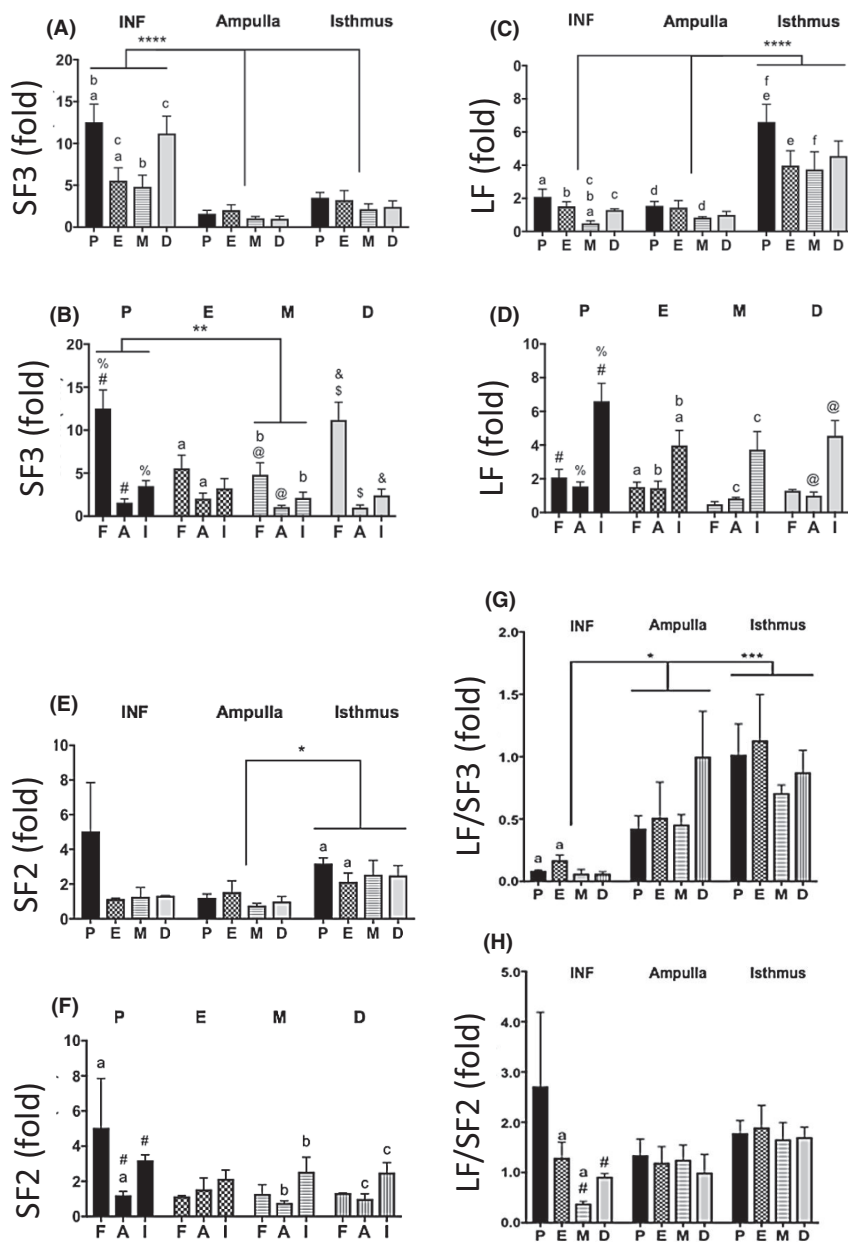


**FIGURE 1** PRLR mRNA expression as a function of oviduct segment and stage of the estrous cycle. SF3 (A, B), LF (C, D), SF2 (E, F), LF/SF3 ratio, (G) and LF/SF2 ratio (H). RT-qPCR  $\Delta\Delta Ct$  values, normalized to *Gapdh* expression ( $\Delta Ct$ ). The Y-axis in (A–F) is fold change, with ampulla in diestrus (set as 1). Infundibular (F), ampullary (A), and isthmic (I) expression grouped by oviduct segment (A, C, E) and stage (B, D, F). Bars: mean fold  $\Delta\Delta Ct$  values  $\pm$  SEM ( $n = 3$ –8 mice, depending on stage, INF data derived from pooled samples). (a–f) lettering denotes pair differences with  $p < 0.05$ , #, %, @, \$, &  $< 0.01$ ; \*\* $p < 0.01$ , \*\*\*\* $p < 0.0001$ )

the ampulla through the proximal isthmus from an animal in proestrus).

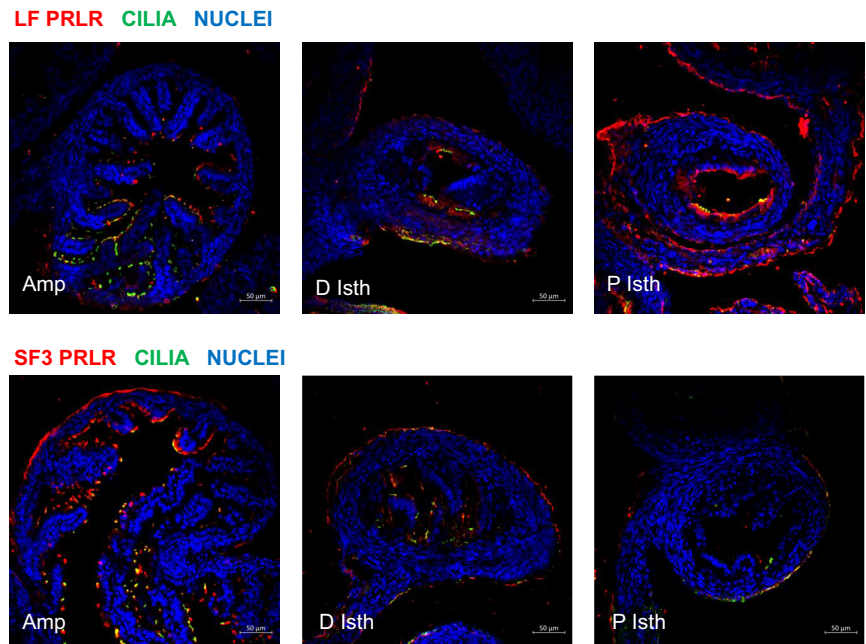
Despite the high expression of SF3 in areas where ciliated cells predominate in the mucosal epithelium and highest expression of LF in areas where secretory cells predominate in the mucosal epithelium, high resolution confocal microscopy showed both LF and SF3 can be on both ciliated and secretory cells throughout the oviduct (Figure 3A,B show examples). Both LF and SF3 clearly localized to the apical border of ciliated and non-ciliated cells. In addition, 3D Imaris Bitplane rendering showed localization of both isoforms on cilia (Movie S1 in supplementary files shows 3D rotation for LF as an example). Thus, although SF3 is most highly expressed in regions where ciliated cells predominate and LF is most highly

expressed in regions where secretory cells predominate, both cell types can have both receptors.

In *Prlr*-IRES-Cre td-Tomato mice that express td-Tomato in cells where the LF *Prlr* has at some time been expressed, patches of td-Tomato+ mucosal epithelial cells were seen in the infundibulum of all mice and throughout the oviduct of some mice (yellow arrows in Figure 4A–D where immunofluorescence localization of td-Tomato fluoresces green). In all mice, many mesothelial (open white arrows) and smooth muscle (open red arrows) cells as well as sporadic cells in the general connective tissue were td-Tomato+. As expected, various structures within the ovary were also highly positive, although the surface epithelium of the ovary was negative.



**FIGURE 2** Immunostaining of PRLRs in the oviduct. Confocal images comparing cross sections of oviduct from ampulla (Amp, left) through distal isthmus (D isth, middle) to proximal isthmus (P Isth, right) at proestrus. Upper panels, LF PRLR; lower panels, SF3 PRLR (both red), together with cilia (acetylated tubulin, green) and nuclei (blue). Bar = 50  $\mu$ M



Expression of *Prlr* in the oviduct was also evaluated by single cell RNA sequencing of oviduct cells dissociated at estrus. Uniform Manifold Approximation and Projection (UMAP) analysis identified nine distinct populations that were classified by their differential gene expression (see Section 2) (Figure 5A,B and Table S1). Expression of *Prlr* was identified in cumulus and mesothelial cells, in addition to a scattering of cells in stromal and smooth muscle populations (Figure 5C) in concordance with our findings by td-Tomato immunofluorescence. However, unlike anti-PRLR immunofluorescence, we detected only a few *Prlr* expressing multi-ciliated cells in epithelial clusters. This discrepancy is likely due to the high dropout rate seen in single cell RNA sequencing datasets as a result of shallow sequencing, which also limits the detection of specific isoforms.<sup>32</sup>

Analysis of whole tubule dissociated cells by flow cytometry demonstrated that epithelial cells (EpCAM+, CD45-) had a greater mean PRLR fluorescence intensity (MFI) than stromal cells (EpCAM-, CD45-), which in turn had a greater MFI than immune cells (EpCAM-, CD45+) (Figure 6A). Because the range of fluorescence was so broad, cells were categorized as low, moderately, or highly positive for LF or SF3. Of the epithelial cells, ciliated cells (EpCAM+, acetylated tubulin+) had more of each type of PRLR (LF or SF3) than non-ciliated cells (Figure 6B,C).

### 3.3 | Signaling through the LF PRLR

Tyrosine phosphorylation of STAT5 is specific to the LF PRLR.<sup>6</sup> For quantification of STAT5 tyrosine phosphorylation, densely ciliated (infundibulum plus ampulla)

and moderate to low ciliated (the isthmus) regions were compared by analyzing areas of mucosa indicated by the red rectangle in the diagrams above the histograms of Figure 7. Controls for the detection of tyrosine phosphorylated STAT5 can be found in Figure S5. An examination of STAT5 tyrosine phosphorylation without any added stimulus showed the greatest endogenous phosphorylation (both apical and basolateral mucosal epithelial) in regions of moderate to low ciliation, as one might expect given the higher expression of LF (Figure 7A,B), although under these circumstances we cannot be sure this is due to PRL as opposed to any other STAT5-tyrosine phosphorylating cytokine. However, in response to a 30-min IP exposure to additional PRL, similarly defined mucosal areas in densely ciliated regions showed substantial tyrosine phosphorylation of STAT5 (Figure 7C,D).

Tyrosine phosphorylated STAT5 appears as puncta and large accumulations of puncta (magnifying the accumulations resolves many individual puncta). Although the merged images suggested that tyrosine phosphorylated STAT5 was in the nucleus, many of the large accumulations were actually extranuclear 30 min after PRL administration (assessed by 3D reconstruction and rotation; Movie S2 shows 3D rotation in supplementary files). Thus, the tyrosine phosphorylated STAT5 is close to the nucleus and, depending on the section may be above or below parts of the nucleus. At this time, it is unclear whether these extranuclear accumulations signify insufficient passage of time from the IP injection to produce complete movement into the nucleus or interaction of tyrosine phosphorylated STAT5 with other molecules in the cytosol that prevent movement into the nucleus. These large tyrosine phosphorylated STAT5 accumulations also

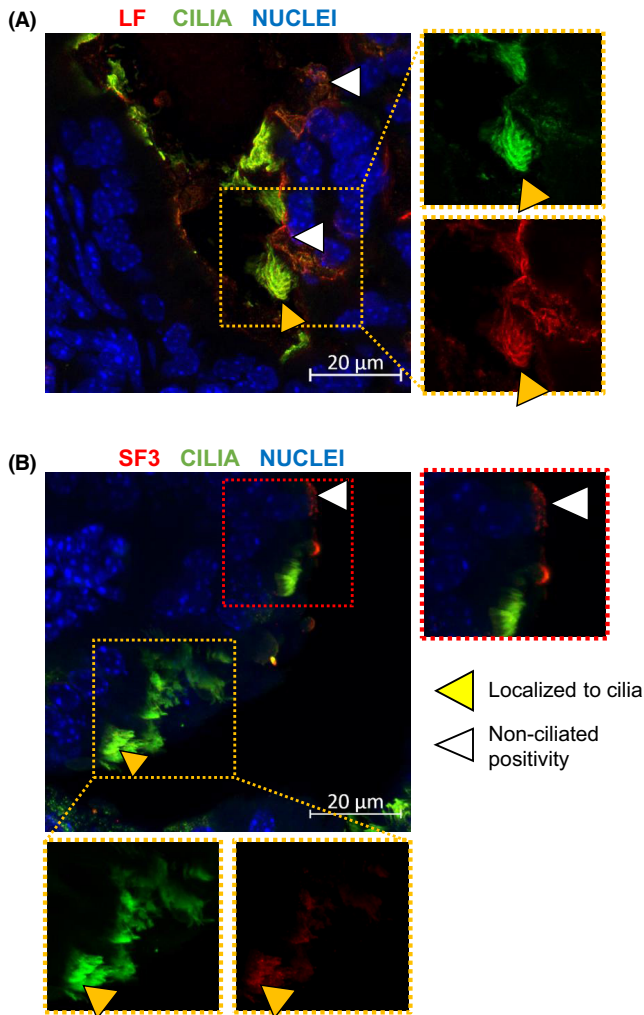


**FIGURE 3** Apical mucosal epithelial localization of LF and SF3 PRLR. High resolution Airyscan confocal imaging of oviduct epithelium, stained for LF (A) or SF3 (B) (both red) at proestrus. Yellow arrowheads denote localization with cilia (green) and white arrowheads denote localization on secretory (non-ciliated) cells. Bars = 20 μm

occurred in the moderately ciliated areas of the isthmus where we observed the ciliated cells to be clustered in trenches between mucosal folds, similar in distribution to the td-Tomato positive cells in the transgenic animals (compare panel 4 D with 7 E).

Regardless of region, 3D Bitplane rendering and masking clearly showed tyrosine phosphorylated STAT5 within cilia (Figure 8). This result confirms the immunofluorescence localization of the LF to cilia and demonstrates receptor signaling through the apical border of ciliated cells.

In proximal regions of the oviduct (defined as areas of moderate to low ciliation), there was a trend toward increased STAT5 tyrosine phosphorylation in response to IP PRL in the smooth muscle, although this did not reach statistical significance (Figure 9). PRL-induced tyrosine phosphorylation of STAT5 in smooth muscle would be

in agreement with the expression of LF mRNA by a proportion of smooth muscle cells, as assessed by single cell RNAseq (Figure 5C). It would also support the results from the transgenic animals that showed smooth muscle cells of the oviduct to be among the most positive for LF expression (Figure 4). However, in the transgenic animals, one cannot determine when the LF *Prlr* was expressed and immunolabeling of the receptors on sections or by flow cytometry showed fewer receptors per cell in smooth muscle/stroma (Figures 2 and 6), a result that correlates with the lower STAT5 tyrosine phosphorylation. In favorable surface grazing sections of the mesothelium, tyrosine phosphorylation of STAT5 could also be appreciated in mesothelial cells (Figure 9B).

### 3.4 | 7-Day treatment with mPRL

Treatment with mPRL for 7 days approximately doubled the median circulating proestrus levels from 35 to 70 ng/mL (Figure S1). While this level is within the lactating physiological range, the mPRL was delivered by Alzet pump and was therefore consistently, rather than episodically, high; thus, it is considered pathological hyperprolactinemia. As evidence that this was sufficient to achieve a biological effect, we examined the mammary gland and found increased expression (fivefold) of *Rankl* and a 50% induction of *Ccnd1* (Figure 6).

Whole transcriptome analysis of infundibula showed 402 genes significantly downregulated and 979 significantly upregulated by mPRL treatment (Figure 10A). Nineteen transcripts showed a  $\log_2$  fold of 1 or greater downregulation, and 15 showed a  $\log_2$  fold of 1 (doubling) or greater upregulation (Figure 10B). While all expression changes are of interest, we have focused on those downregulated a fold or greater in response to PRL treatment, in part because the list contains several genes that identify the cell type being affected. Of note, we identified downregulated genes associated with multi-ciliogenesis, including *Mcidas* (also known as multicilin), *Panx2* (Pannexin 2), and *Cdc20b* (Cell division cycle 20b). Downregulation of *Mcidas* was confirmed by RT-qPCR (Figure 10C).

PRL also reduced expression of several genes associated with the oocyte and developing embryo. Thus, mRNA for zona pellucida binding protein 2, *Zbp2*, zona pellucida glycoprotein 3, *Zp3*, and NLR family, pyrin domain containing 5, *Nlrp5* or *Mater*, are each involved in successful development or survival of the oocyte.<sup>33,34</sup> The depth of sequencing (>80 million reads per sample) also allowed us to examine splice variants. Of interest to the current manuscript was a lack of effect of PRL treatment on *Prlr* expression or splicing. A lack of effect on LF mRNA expression was confirmed by RT-qPCR (Figure 10C).

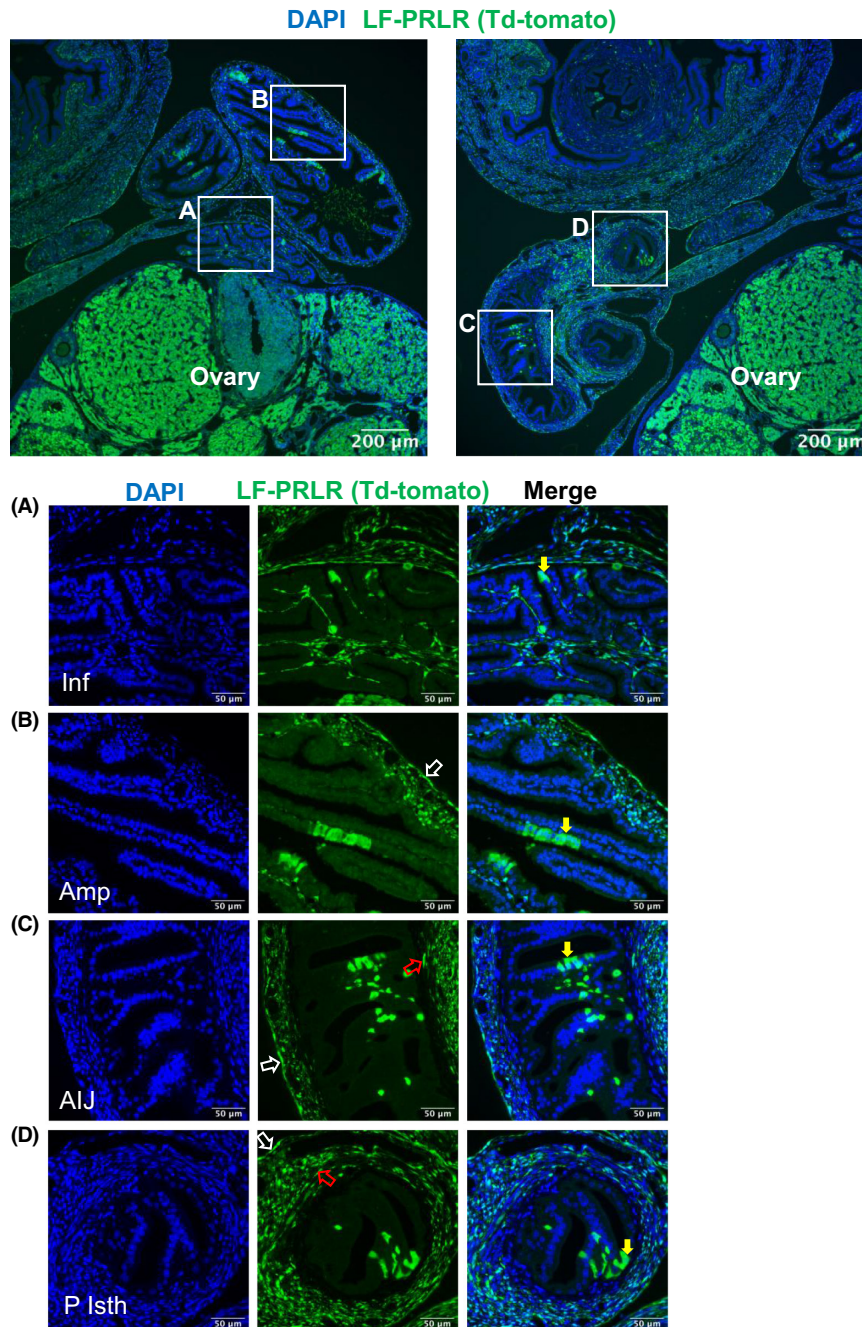


**FIGURE 4** Expression of LF PRLR in oviduct of *Prlr* IRES-Cre td-Tomato mice as determined by immunostaining for td-Tomato. (A–D) High power images of boxed areas (white) in low power images showing LF expression (td-Tomato, green) and nuclei (DAPI, blue) in different regions of the oviduct at proestrus. (A) td-Tomato immunofluorescence showing LF expression in some epithelial cells and in the stroma of the infundibulum. (B) Clusters of LF+ epithelial cells and positive expression in the smooth muscle layer in the ampulla. Positive immunofluorescence for LF is also evident in the general stroma. (C) The ampulla/isthmic junction where LF expressing cells are dispersed throughout the smooth muscle layer. Single LF+ epithelial cells are scattered throughout the mucosal epithelium. No expression was detected in the stroma. (D) In the proximal isthmus, widespread positive LF expression is evident in the smooth muscle layer. LF-containing cells in the epithelial layer show a similar scattered distribution as that seen in C. Inf, Infundibulum; Amp, Ampulla; AIJ, Ampulla/Isthmic Junction; P Isth, Proximal Isthmus. Solid yellow arrows indicate examples of LF expression by mucosal epithelium, open white arrows examples in mesothelium and open red arrows, examples in smooth muscle. Bars are 200  $\mu$ m in low magnification views and 50  $\mu$ m in (A–D)

## 4 | DISCUSSION

In this study, we have applied multiple different approaches to begin to understand the role PRL may play

in the oviduct. Each approach has its limitations (specificity, sensitivity, ontogeny, as well as detection of either mRNA or protein) but collectively the results provide evidence from more than one approach that PRLRs are

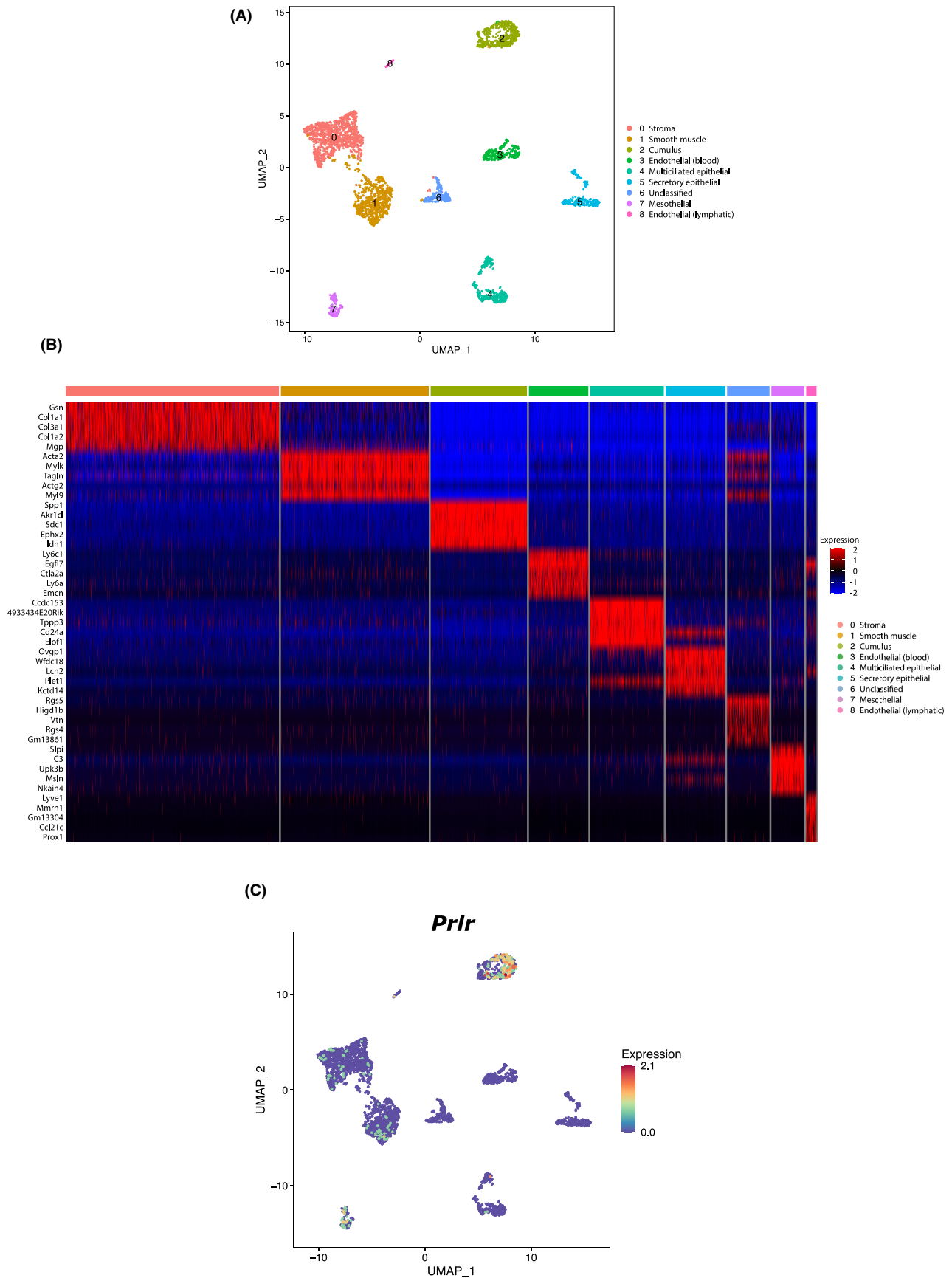


**FIGURE 5** *Prlr* expression in the oviduct as determined by single cell RNAseq. Cells were isolated from a single mouse in estrus. UMAP clustering segregated oviduct cells into nine distinct populations (A). A heat map of the top differentially expressed genes within each cluster (see Table S1 for complete list) (B). A heat map showing the expression of *Prlr* across clusters (C)

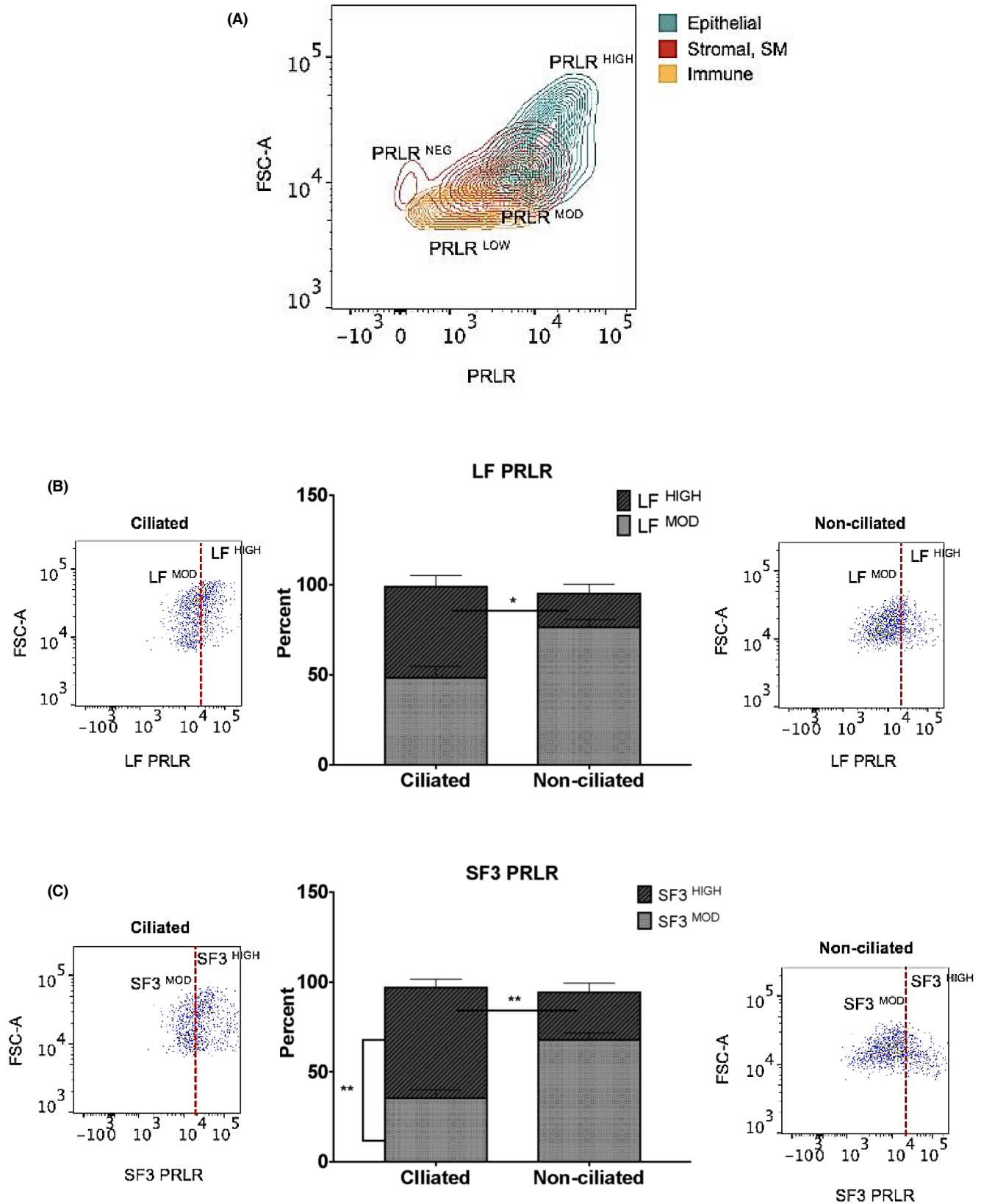
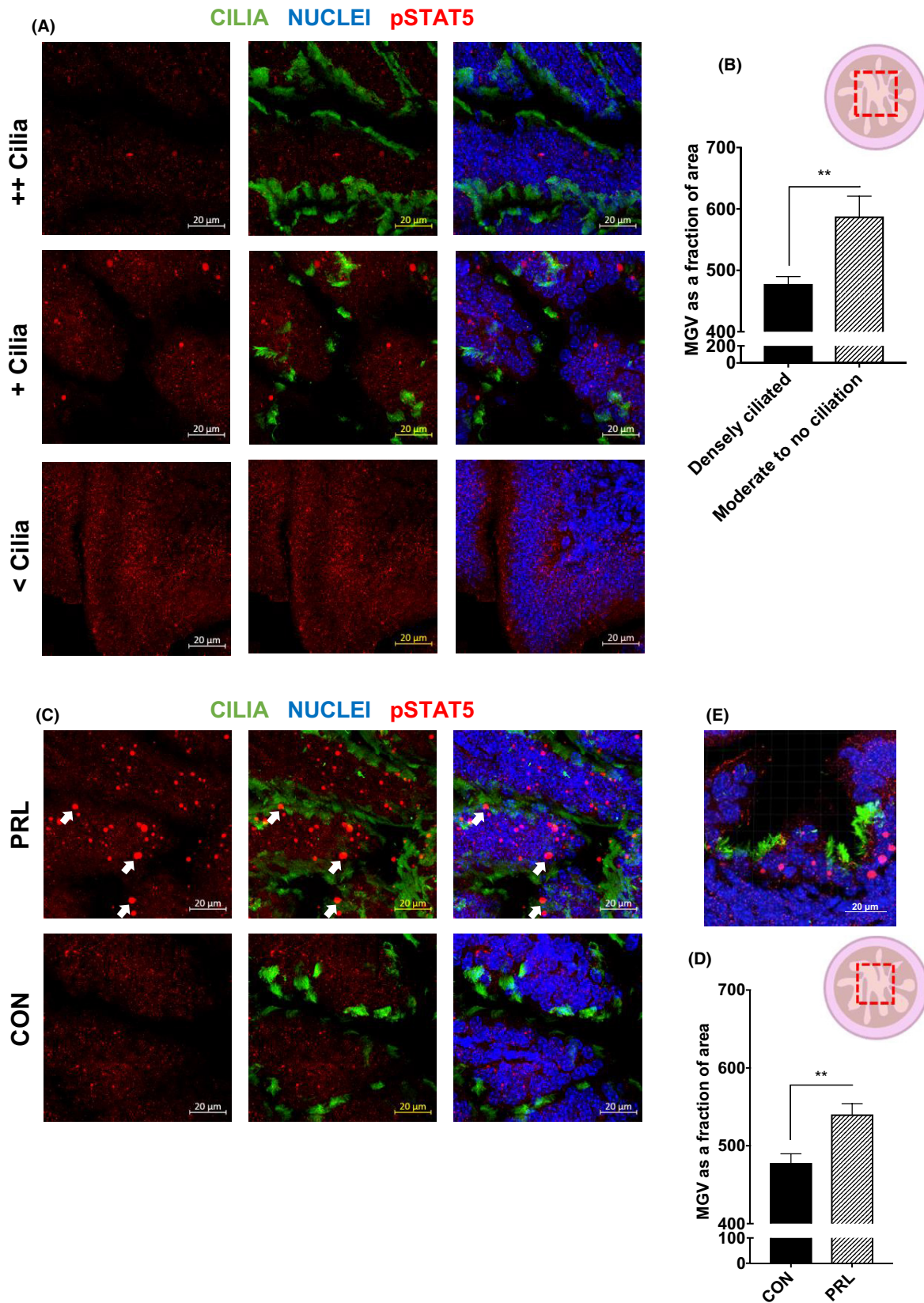


**FIGURE 6** PRLR expression by oviduct cells analyzed by flow cytometry. Gating to obtain epithelial, smooth muscle/stromal, and immune populations are shown in Figure S4. Subsequently, cells were categorized as negative (NEG), low, moderate (MOD), or high expressors of PRLR (A) and moderate to high expressors of either LF (B) or SF3 (C) as a function of their ciliated (acetylated tubulin +ve) or non-ciliated status. Histograms show the mean  $\pm$  SEM of triplicates derived from pooled cells from 16 adult females taken separately through staining. \* $p < 0.05$ , \*\* $p < 0.01$



expressed by mucosal epithelial, smooth muscle, and mesothelial cells. Thus, for example, regional differences in the relative quantities of SF3 and LF mRNAs seen by

tissue RT-qPCR were in good agreement with what was observed by antibody labeling of both the mucosal epithelium and mesothelium. Mesothelial expression of PRLRs

**FIGURE 7** Tyrosine phosphorylated STAT5 without and with acute elevation of PRL. Images of equivalent areas from regions densely ciliated ( $++$ cilia), moderately ciliated ( $+cilia$ ), and sparsely- no ciliation ( $<cilia$ ) in the oviduct showing phospho-STAT5 (pSTAT5, red), cilia (green), and nuclei (blue) with quantification comparing the relative degree of tyrosine phosphorylation without added PRL in densely ciliated (infundibulum and ampulla) versus moderate to low ciliated (isthmus) areas (A&B). Images of equivalent areas in a densely ciliated region without (CON) and with (PRL) IP injection of PRL and quantification of the difference in terms of tyrosine phosphorylated STAT5 (C&D). Panel E shows a ciliated area in a mucosal trench in the isthmus in response to added PRL. All animals used for analysis of STAT5 phosphorylation in this and subsequent figures were in diestrus since this is when circulating PRL levels are low and added PRL would be expected to make the largest difference. Bars = 20  $\mu$ m. The diagrams above histograms show the areas quantified in B and D (red rectangle).  $n = 5$  animals per group with three images per frozen section. Histograms show mean  $\pm$  SEM.  $**p < 0.01$

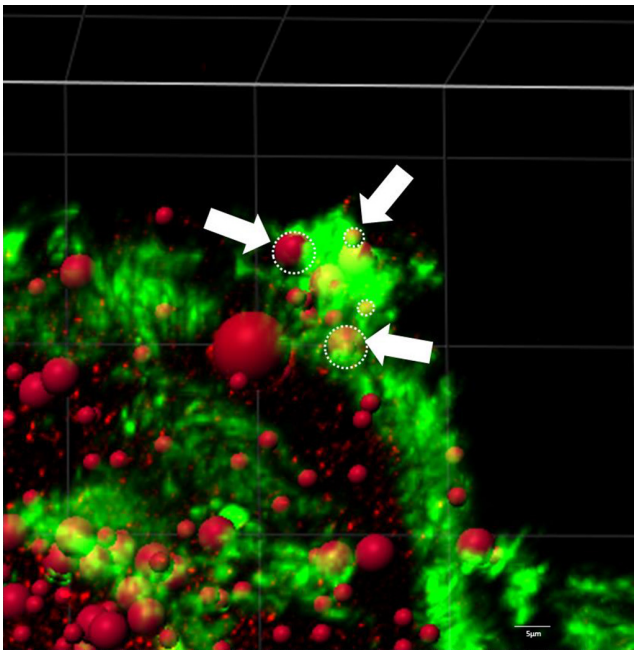


**FIGURE 8** Localization of phospho-STAT5 within cilia/ciliated cells. 3D Imapris Bitplane rendering of confocal images of oviduct epithelium stained with anti-pSTAT5. pSTAT5 puncta (red) were masked to highlight localization. White arrows and dotted circles show examples of localization of pSTAT5 to ciliated border (cilia in green). Bar = 5  $\mu$ m

was also seen by single cell RNAseq and in the transgenic animals. For the mucosal epithelium, the presence of the LF was also observed in patches throughout the oviduct in some of the transgenic animals and further demonstrated by PRL tyrosine phosphorylation of STAT5. Expression of LF PRLR by smooth muscle cells was seen in the transgenic animals and supported by the trend in STAT5 tyrosine phosphorylation in response to IP PRL, and also by the presence of some form of the PRLR, as determined by single cell RNAseq.

Only a single study has previously examined PRLR expression in the murine oviduct and human fallopian tube.<sup>13</sup> These authors reported the presence of both long and short receptors analyzed by western blot, and apical localization of an unidentified form of PRLR on the mucosal epithelium by immunostaining. While trailblazing,

this initial study was limited in scope by not identifying which short forms were expressed and by not distinguishing among the different functional regions of the oviduct or by stage of the estrous cycle, the latter since they examined either neonatal or ovariectomized animals. We therefore began the current study by analyzing expression of all four mouse PRLR isoforms as a function of oviduct segment and stage of the estrous cycle. This approach has its limitations since expression at the mRNA level may or may not be directly reflective of protein expression. However, when the relative abundance of the two most highly expressed forms, LF and SF3, was compared at the mRNA and protein level as a function of segment of the oviduct, there was coordinated expression. That is the mRNA for SF3 and immunostaining for SF3 was greatest in densely ciliated areas and mRNA for LF and immunostaining for LF was greatest in areas of moderate to low ciliation.

Hormones of the estrous cycle influence the function of the oviduct,<sup>35,36</sup> but it is essentially only in the infundibulum that these hormones affected PRLR transcript levels. As a result, the LF/SF3 mRNA ratio almost doubles during estrus, mostly due to a reduction in SF3. Based on the 7-day treatment with PRL, it does not seem to be PRL regulating SF3 expression since PRL treatment did not change PRLR mRNA expression or pre-mRNA splicing. Given the rapidity of murine estrous cycles, it seems likely that the hormones changing in proestrus would be responsible for the decrease in SF3 seen in estrus and metestrus. Besides PRL, these include an increase in estradiol, follicle stimulating hormone and luteinizing hormone and a decrease in both inhibins A and B.<sup>37,38</sup> It will therefore take some time to determine which of these hormones regulates *Prlr* transcription rate, pre-mRNA splicing, transcript degradation, translation, and/or protein degradation in the infundibulum. Nevertheless, since PRL itself does not regulate expression of PRLRs, estrous cycle regulation of specific PRLR isoform expression supports a cyclic change in the function of PRL in the infundibulum, with stable functions for PRL elsewhere in the oviduct. In the infundibulum, the predominant cell type is multiciliated and ciliary motility<sup>39</sup> and binding of cumulus cells to sequential cilia<sup>40</sup> are crucial for oocyte pickup. We

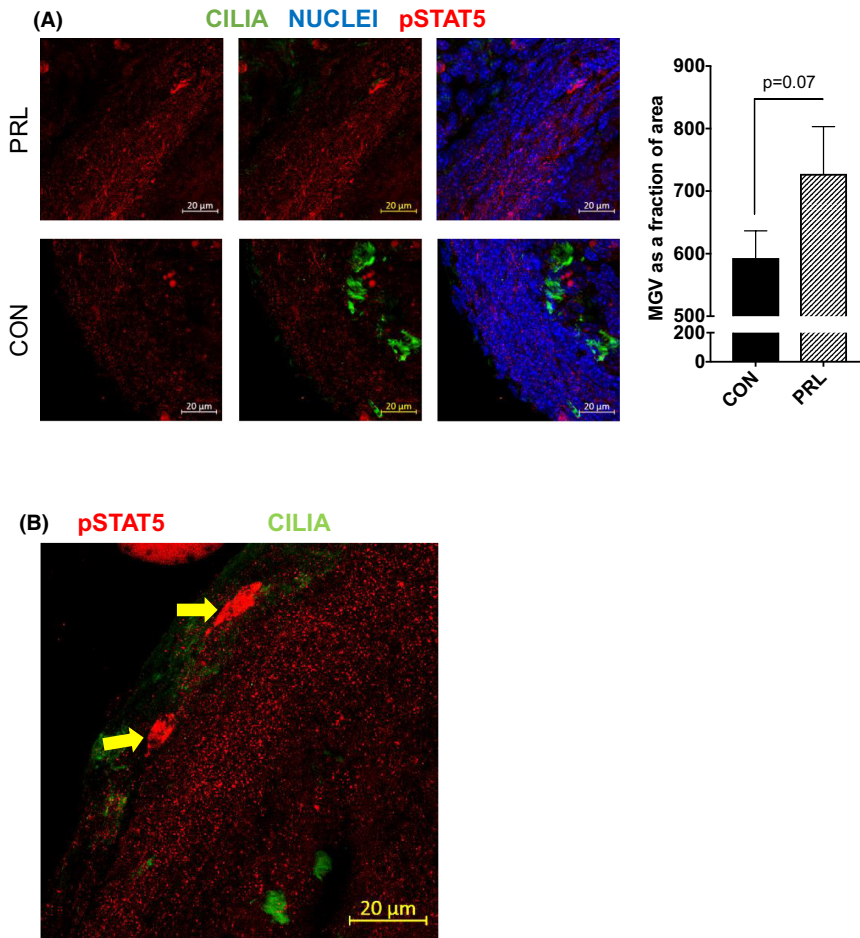


**FIGURE 9** STAT5 tyrosine phosphorylation in smooth muscle and mesothelium. Confocal imaging of sections stained for phospho-STAT5 (red), cilia (green), and nuclei (blue) in areas of low to no ciliation in PRL-treated (PRL) versus control (CON) animals (A). Smooth muscle can be recognized by the densely packed and ordered nuclei.  $n = 5$  animals per group with three images per section. Histograms show mean  $\pm$  SEM. A higher magnification view of tyrosine phosphorylated STAT5 (red) in mesothelium (arrows in B where green is cilia). Bars = 20  $\mu$ m

speculate therefore that a decrease in SF3 expression may be important for organized ciliary beating or ciliary crown placement of adhesive substances.

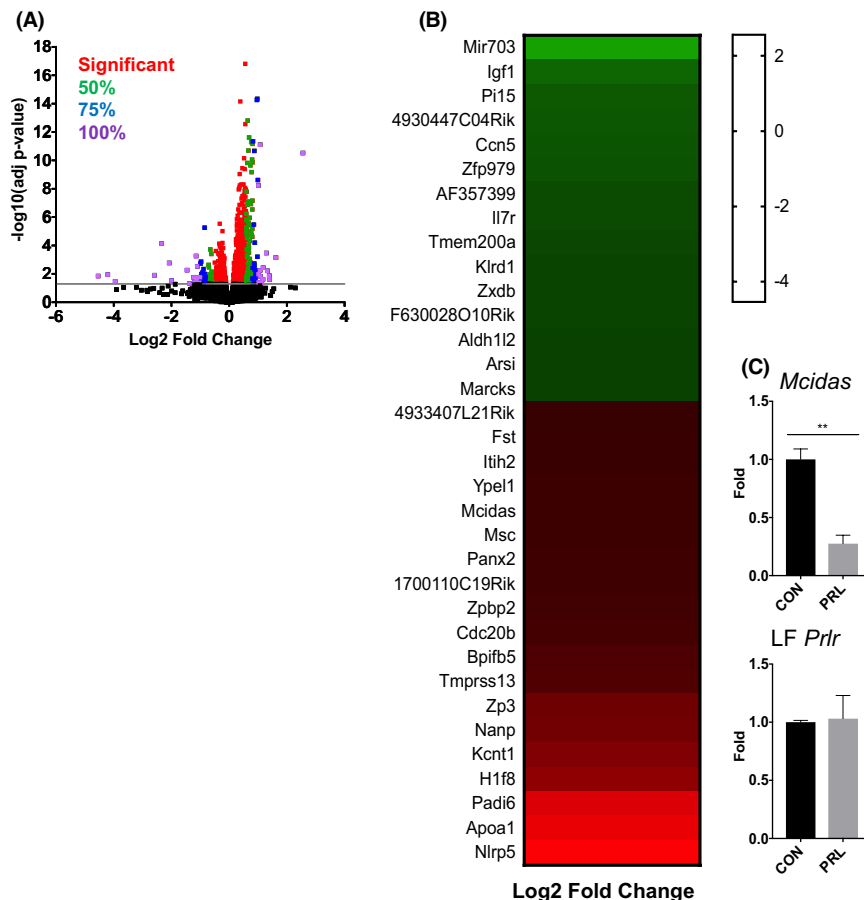
Both SF3 and LF PRLR localize to cilia and one can see STAT5 tyrosine phosphorylation within cilia, thereby suggesting that the PRL to which these receptors are responding is within the oviduct. Experimentally, this would have come from the peritoneal fluid through the bursal foramen.<sup>41</sup> Physiologically, the PRL could also be delivered via this route, could be a transudate from plasma, or could come from follicular fluid or cells of the ovulated mass.<sup>42,43</sup> No production of PRL by oviduct cells was detected by either single cell RNAseq or RT-qPCR of the individual segments (negative data not presented) and so the PRLRs are not responding to autocrine/paracrine PRL. The *Prlr* expression in cumulus cells, which was observed in the current study by single cell RNAseq, and known effects of PRL on fertilization and embryo maturation,<sup>44</sup> support the presence and importance of PRL in oviductal fluid.

The RNAseq data from prolonged elevated PRL (analyzed at proestrus) show effects on at least three multi-ciliated cell-specific genes.<sup>45</sup> While these particular responses are more likely reflective of prolonged hyperprolactinemia, together with the demonstration of PRLR on, and tyrosine phosphorylation of STAT5

within, ciliated cells, they nevertheless support effects of PRL on ciliated cells. Downregulation of *Mcidas*, *Panx2*, and *Cdc20b* would be expected to reduce the function and differentiated state of existing ciliated cells and/or prevent the formation of new ciliated cells. *Mcidas* is one of the two known major upstream activators of the multi-ciliated cell transcriptional program.<sup>45</sup> Pannexins are epithelial channel proteins that contribute to ATP release into the extracellular space. ATP release, in turn, increases ciliary beat frequency.<sup>46,47</sup> *Cdc20b* is required for deuterosome-mediated centriole production in vertebrate multi-ciliated cells.<sup>48</sup> With reduced ciliation/reduced ciliary function one would expect less efficient ovum transport<sup>40</sup> and alterations in fluid microenvironments,<sup>45</sup> both of which would negatively impact fertility. Since human growth hormone also interacts with the human PRLR,<sup>49</sup> there is the potential for clinical conditions of growth hormone excess to have similar negative impacts on fertility. Changes in gene expression with prolonged hyperprolactinemia also demonstrated the presence of ova in the infundibulum samples. This further suggests a detrimental effect of hyperprolactinemia on ovum transport further into the oviduct. The negative impact of hyperprolactinemia on the ovum-specific genes themselves is hard



**FIGURE 10** Differentially expressed genes in the infundibulum following the 7-day PRL treatment. Volcano plot with  $\log_2$  fold change on the  $x$ -axis of all differentially expressed genes (control vs. PRL treatment). Significance threshold set at FDR adjusted  $p$ -value (adj.  $p$ -value)  $\leq 0.05$  (red), those up- or downregulated by 50% (green), by 75% (blue) or by 100% or more (violet) (A). Tabulation of those upregulated by a fold or more (green) and downregulated a fold or more (red) with depth of color indicating log base twofold change in control versus PRL-treated animals.  $n = 5$  samples per group, with two animals per sample (four infundibula) (B). RT-qPCR of *Mcidas* and *LF Prlr* in the same samples (C). Values normalized to *Gapdh* expression ( $\Delta\text{Ct}$ ). The Y-axis is fold change normalized to control group ( $\Delta\Delta\text{Ct}$ , set as 1).  $n = 3$ ,  $**p < 0.01$



to further interpret since it could indicate effects prior to ovulation or effects reflective of a less than optimal environment in the oviduct.

Localization of PRLR to mesothelial cells was originally an unexpected finding. However, close inspection of the images in Aoki et al.<sup>14</sup> also shows fluorescence indicative of expression of the LF in mesothelial cells. Totally unexpected was coordinated relative expression of SF3 and LF on mesothelium with the mucosal epithelium in the different segments of the oviduct. The mesothelium is responsible for maintenance of a slippery surface on organs in various body cavities, initiation of immune/inflammatory responses to foreign antigens,<sup>50</sup> and for regulation of ion and fluid transport by a variety of means, including intercellular and transcellular transport.<sup>51,52</sup> PRL certainly regulates ion and fluid transport in a variety of other tissues, including renal tubule cells and epithelial cells of the lactating mammary gland.<sup>53,54</sup> Perhaps PRL acting through specific PRLR isoforms is important to differential fluid and ion transport in densely ciliated areas versus those with moderate to low ciliation. PRL certainly is important to fluid flow in the oviduct that governs sperm rheotaxis.<sup>55</sup>

PRLRs and maybe some tyrosine phosphorylation of STAT5 in response to acutely elevated PRL was also seen

in the smooth muscle of the oviduct. This was not unexpected since Aoki et al.<sup>14</sup> had previously demonstrated LF expression in the smooth muscle of the oviduct. However, in their study, which used a transgenic animal that expressed tauGFP in all cells that expressed the LF *Prlr* and in the current study where td-Tomato was used for the same purpose, positivity seems much greater in the smooth muscle than the mucosal epithelium, whereas the current immunostaining, flow cytometry, and tyrosine phosphorylation of STAT5 data suggest a lower level of LF expression in smooth muscle versus mucosal epithelium. Since cells in the transgenic animals would be GFP+ or td-Tomato+ from expression at any time during development, this suggests that PRL, working through the LF, may be more important in smooth muscle during development of the oviduct than it is in the adult. Alternatively, it may represent a difference in expression of mRNA versus protein. In the adult, acute tyrosine phosphorylation of STAT5 was detectable in smooth muscle in regions of moderate to low ciliation, perhaps suggesting a greater role for PRL in regulating smooth muscle function in proximal regions of the oviduct. Certainly, there are differences in smooth muscle morphology and function between the proximal and distal oviduct.<sup>35</sup>

In conclusion, this work supports a previous demonstration of PRLR expression by mucosal epithelial cells in the oviduct and adds to the previous findings by also demonstrating expression by oviductal mesothelial and smooth muscle cells. Analysis of expression of the differentially spliced forms of the PRLR suggests that PRL has different activities in the infundibulum, ampulla, and isthmus, with those in the infundibulum changed as a function of the estrous cycle. Analysis of signaling through the LF clearly identified ciliated cells as responsive to acute elevations in PRL. In addition, the gene expression studies showed that prolonged hyperprolactinemia would negatively impact ciliated cell function, thereby providing a novel additional mechanism whereby hyperprolactinemia would reduce fertility.

### ACKNOWLEDGMENTS

The authors thank Dr. Emma Wilson, University of California, Riverside, for access to the Canto Flow cytometer and Wilson lab members for help in trouble shooting the flow cytometry experiments. The authors also thank Dr. David Carter of the Microscopy and Imaging Core Facility, University of California, Riverside, for assistance with the Zeiss high resolution Airyscan imaging. The authors thank the Otago Histology Services unit, Dept of Pathology, University of Otago for assistance with paraffin embedding and sectioning oviduct tissue from *Prlr*-IRES-Cre td-Tomato mice.

This work was primarily supported by research funds awarded to AMW for service as Vice Provost. KCR was partially supported by the Pease Cancer and Mary Galvin Burden Pre-Doctoral Fellowships, a Graduate Council Dissertation Research Grant and a Graduate Division Dissertation Year Award. MJF was supported by Canderel, CRRD, and FRQS postdoctoral fellowships. HRP was supported by a grant administered through the Neurological Foundation of New Zealand. The Genomics High Throughput Facility at the University of California, Irvine, which conducted the tissue RNAseq, is supported in part by Cancer Center Support Grant (P30CA-062203) and National Institutes of Health shared instrumentation grants 1S10RR025496-01, 1S10OD010794-01, and 1S10OD021718-01.

### CONFLICT OF INTEREST

All authors declare that there is no conflict of interest that could be perceived as prejudicing the impartiality of the research reported.

### AUTHOR CONTRIBUTIONS

Different aspects of the research were designed by all authors; KCR, AMW, MJF, and HRP performed the experiments; all authors analyzed data; members of all

three groups contributed to the writing, and the manuscript was subsequently edited and finally approved by all authors.

### ORCID

David R. Grattan  <https://orcid.org/0000-0001-5606-2559>

Ameae M. Walker  <https://orcid.org/0000-0002-7614-7450>

### REFERENCES

1. Stewart CA, Behringer RR. Mouse oviduct development. In: Kubiak JZ, ed. *Mouse Development: From Oocyte to Stem Cells*. Springer; 2012:247-262.
2. Stewart CA, Behringer RR. Mouse oviduct development. *Results Probl Cell Differ*. 2012;55:247-262.
3. Boutin JM, Edery M, Shiota M, et al. Identification of a cDNA encoding a long form of prolactin receptor in human hepatoma and breast cancer cells. *Mol Endocrinol*. 1989;3:1455-1461.
4. Hu ZZ, Meng JP, Dufau ML. Isolation and characterization of two novel forms of the human prolactin receptor generated by alternative splicing of a newly identified exon 11. *J Biol Chem*. 2001;276:41086-41094.
5. Tzeng SJ, Linzer DI. Prolactin receptor expression in the developing mouse embryo. *Mol Reprod Dev*. 1997;48:45-52.
6. Ben-Jonathan N, LaPensee CR, LaPensee EW. What can we learn from rodents about prolactin in humans? *Endocr Rev*. 2008;29:1-41.
7. Devi YS, Shehu A, Stocco C, et al. Gibori G regulation of transcription factors and repression of Sp1 by prolactin signaling through the short isoform of its cognate receptor. *Endocrinology*. 2009;150:3327-3335.
8. Devi YS, Seibold AM, Shehu A, et al. Inhibition of MAPK by prolactin signaling through the short form of its receptor in the ovary and decidua: involvement of a novel phosphatase. *Biol Chem*. 2011;286:7609-7618.
9. Huang K, Ueda E, Chen Y, Walker AM. Paradigm-shifters: phosphorylated prolactin and short prolactin receptors. *J Mammary Gland Biol Neoplasia*. 2008;13:69-79.
10. Tan DY, Walker AM. Short form 1b human prolactin receptor down-regulates expression of the long form. *J Mol Endocrinol*. 2010;44:187-194.
11. Trott JF, Hovey RC, Koduri S, Vonderhaar BK. Alternative splicing to exon 11 of human prolactin receptor gene results in multiple isoforms including a secreted prolactin-binding protein. *J Mol Endocrinol*. 2003;30:31-47.
12. Bole-Feysot C, Goffin V, Edery M, Binart N, Kelly PA prolactin (PRL) and its receptor: actions, signal transduction pathways and phenotypes observed in PRL receptor knockout mice. *Endocr Rev*. 1998;19:225-268.
13. Shao R, Nutu M, Weijdegård B, et al. Differences in prolactin receptor (PRLR) in mouse and human fallopian tubes: evidence for multiple regulatory mechanisms controlling PRLR isoform expression in mice. *Biol Reprod*. 2008;79:748-757.
14. Aoki M, Wartenberg P, Grünwald R, et al. Widespread cell-specific prolactin receptor expression in multiple murine organs. *Endocrinology*. 2019;160:2587-2599.

15. Clevenger CV, Chang WP, Ngo W, Pasha TL, Montone KT, Tomaszewski JE. Expression of prolactin and prolactin receptor in human breast carcinoma – evidence for an autocrine paracrine loop. *Am J Pathol.* 1995;146:695-705.
16. Freeman ME, Kanyicska B, Lerant A, Nagy G. Prolactin: structure, function, and regulation of secretion. *Physiol Rev.* 2000;80:1523-1631.
17. Michael SD. Plasma prolactin and progesterone during the estrous cycle in the mouse. *Proc Soc Exp Biol Med.* 1976;153:254-257.
18. Phillipps HR, Khant Aung Z, Grattan DR. Elevated prolactin secretion during proestrus in mice: absence of a defined surge. *J Neuroendocrinol.* 2022. <https://doi.org/10.1111/jne.13129>
19. Caligioni CS. Assessing reproductive status/stages in mice. *Curr Protoc Neurosci.* 2009;48:A.4I.1-A.4I.8.
20. Radecki KC, Lorenson MY, Carter DG, Walker AM. Microdissection and dissociation of the murine oviduct: individual segment identification and single cell isolation. *J Vis Exp.* 2021;177:e63168.
21. Chen TJ, Kuo CB, Tsai KF, Liu JW, Chen DY, Walker AM. Development of recombinant human prolactin receptor antagonists by molecular mimicry of the phosphorylated hormone. *Endocrinology.* 1998;139:609-616.
22. Huang KT, Chen YH, Walker AM. Inaccuracies in MTS assays: major distorting effects of medium, serum albumin, and fatty acids. *BioTechniques* 2004; 37 406, 408 410–412.
23. Martin TJ, Gillespie MT. Receptor activator of nuclear factor  $\kappa$ B ligand (RANKL): another link between breast and bone. *Trends Endocrinol Metab.* 2001;12:2-4.
24. Kokay I, Wyatt A, Phillipps H, et al. Analysis of prolactin receptor expression in the murine brain using a novel prolactin receptor reporter mouse. *J Neuroendocrinol.* 2018;30:e1263.
25. Livak KJ, Schmittgen TD. Analysis of relative gene expression data using real-time quantitative PCR and the  $2^{-\Delta\Delta CT}$  method. *Methods.* 2001;25:402-408.
26. Ueda EK, Huang K, Nguyen V, Ferreira M, Andre S, Walker AM. Distribution of prolactin receptors suggests an intraductal role for prolactin in the mouse and human mammary gland, a finding supported by analysis of signaling in polarized monolayer cultures. *Cell Tissue Res.* 2011;346:175-189.
27. Sellitti DF, Akamizu T, Doi SQ, et al. Renal expression of two 'thyroid-specific' genes: thyrotropin receptor and thyroglobulin. *Nephron Exp Nephrol.* 2000;8:235-243.
28. Huff J. The Airyscan detector from ZEISS: confocal imaging with improved signal-to-noise ratio and super-resolution. *Nat Methods.* 2015;12:i-ii.
29. Ford MJ, Harwalkar K, Pacis AS, et al. Oviduct epithelial cells constitute two developmentally distinct lineages that are spatially separated along the distal-proximal axis. *Cell Rep.* 2021;36:109677.
30. Love MI, Soneson C, Patro R. Swimming downstream: statistical analysis of differential transcript usage following Salmon quantification. *F1000Res.* 2018;7:952.
31. Grubbs F. Procedures for detecting outlying observations in samples. *Dent Tech.* 1969;11:1-21.
32. Svensson V, Natarajan KN, Ly LH, et al. Power analysis of single-cell RNA-sequencing experiments. *Nat Methods.* 2017;14:381-387.
33. Gupta SK, Bhandari B, Shrestha A, et al. Mammalian zona pellucida glycoproteins: structure and function during fertilization. *Cell Tissue Res.* 2012;349:665-678.
34. Tong ZB, Gold L, Pfeifer KE, et al. Mater, a maternal effect gene required for early embryonic development in mice. *Nat Genet.* 2000;26:267-268.
35. Faussonne-Pellegrini MS, Bani G. The muscle coat morphology of the mouse oviduct during the estrous cycle. *Arch Histol Cytol.* 1990;53:167-178.
36. Roberson EC, Battenhouse AM, Garge RK, Tran NK, Marcotte EM, Wallingford JB. Spatiotemporal transcriptional dynamics of the cycling mouse oviduct. *Dev Biol.* 2021;476:240-248.
37. Hawkins SM, Matzuk MM. The menstrual cycle: basic biology. *Ann NY Acad Sci.* 2008;1135:10-18.
38. Parkening TA, Collins TJ, Smith ER. Plasma and pituitary concentrations of LH, FSH and prolactin in aging C57Bl/6 mice at various times of the estrous cycle. *Neurobiol Aging.* 1982;3:31-35.
39. Yuan S, Wang Z, Peng H, et al. Oviductal motile cilia are essential for oocyte pickup but dispensable for sperm and embryo transport. *Proc Natl Acad Sci USA.* 2021;118:e2102940118.
40. Lam X, Gieseke C, Knoll M, Talbot P. Assay and importance of adhesive interaction between hamster (*Mesocricetus auratus*) oocyte-cumulus complexes and the oviductal epithelium. *Biol Reprod.* 2000;62:579-588.
41. Hosotani M, Ichii O, Nakamura T, et al. Anatomy and histology of the foramen of ovarian bursa opening to the peritoneal cavity and its changes in autoimmune disease-prone mice. *J Anat.* 2021;238:73-85.
42. Phelps JY, Bugg EM, Shablott MJ, Vlahos NP, Whelan J, Zacur HA. Prolactin gene expression in human ovarian follicular cells. *Fertil Steril.* 2003;79:182-185.
43. Kiapekou E, Loutradis D, Mastorakos G, et al. Effect of PRL on in vitro follicle growth, in vitro oocyte maturation, fertilization and early embryonic development in mice. *Cloning Stem Cells.* 2009;11:293-300.
44. Spassky N, Meunier A. The development and functions of multiciliated epithelia. *Nat Rev Mol Cell Biol.* 2017;18:423-436.
45. Ohbuchi T, Suzuki H. Synchronized roles of pannexin and connexin in nasal mucosal epithelia. *Eur Arch Otorhinolaryngol.* 2018;275:1657-1661.
46. Ransford GA, Fregien N, Qiu F, Dahl G, Conner GE, Salathe M. Pannexin 1 contributes to ATP release in airway epithelia. *Am J Respir Cell Mol Biol.* 2009;41:525-534.
47. Revinski DR, Zaragosi LE, Boutin C, et al. CDC20B is required for deuterosome-mediated centriole production in multiciliated cells. *Nat Commun.* 2018;9:4668.
48. Cunningham BC, Bass S, Fuh G, Wells JA. Zinc mediation of the binding of human growth hormone to the human prolactin receptor. *Science.* 1990;250:1709-1712.
49. Mutsaers SE, Prêle CM, Pengelly S, Herrick SE. Mesothelial cells and peritoneal homeostasis. *Fertil Steril.* 2016;106:1018-1024.
50. Isaza-Restrepo A, Martin-Saavedra JS, Velez-Leal JL, Vargas-Barato F, Riveros-Dueñas R. The peritoneum: beyond the tissue – a review. *Front Physiol.* 2018;9:738.
51. Ji H-L, Nie HG. Electrolyte and fluid transport in mesothelial cells. *J Epithelial Biol Pharmacol.* 2008;1:1-7.
52. Greenlee MM, Mitzelfelt JD, Duke BJ, Al-Khalili O, Bao HF, Eaton DC. Prolactin stimulates sodium and chloride ion channels in A6 renal epithelial cells. *Am J Physiol Ren Physiol.* 2015;308:F697-F705.
53. Shennan DB, Peaker M. Transport of milk constituents by the mammary gland. *Physiol Rev.* 2000;80:925-951.

54. Miki K, Clapham DE. Rheotaxis guides mammalian sperm. *Curr Biol*. 2013;23:443-452.
55. Marano RJ, Ben-Jonathan N. Minireview: Extrapituitary prolactin: an update on the distribution, regulation, and functions. *Mol Endocrinol*. 2014;28:622-633.

**How to cite this article:** Radecki KC, Ford MJ, Phillipps HR, et al. Multiple cell types in the oviduct express the prolactin receptor. *FASEB BioAdvances*. 2022;4:485-504. doi: [10.1096/fba.2022-00004](https://doi.org/10.1096/fba.2022-00004)

### SUPPORTING INFORMATION

Additional supporting information may be found in the online version of the article at the publisher's website.